iJRASET
International Journal For Research in Applied Science and Engineering Technology

INTERNATIONAL JOURNAL FOR RESEARCH

IN APPLIED SCIENCE & ENGINEERING TECHNOLOGY

Volume: 6 **Issue:** XII **Month of publication:** December 2018

DOI:

www.ijraset.com

Call: 08813907089 | E-mail ID: ijraset@gmail.com

International Journal for Research in Applied Science & Engineering Technology (IJRASET)
ISSN: 2321-9653; IC Value: 45.98; SJ Impact Factor: 6.887
Volume 6 Issue XII, Dec 2018- Available at www.ijraset.com

Structural and Electrical Properties of Ytterbium and Samarium Co-Doped Ceria as a Solid Electrolyte for Intermediate-Temperature Solid Oxide Fuel Cell

Lemessa Asefa Eressa[1], PV Bhaskara Rao[2]
[1, 2]*Wollega University, Department of Physics, Nekemte, Ethiopia.*

Abstract: ***Co-doped samples of electrolytes $Ce_{1-x-y}Sm_xYb_yO_{2-\delta}$, $(x = 0.05, y = 0.05, 0.1)$, have been prepared by Sol- gel method and characterized to explore their use as a solid electrolyte for intermediate temperature solid oxide fuel cells (IT-SOFCs). The crystal structure, microstructure, and ionic conductivity have been determined by X-ray diffraction (XRD), Scanning electron microscopy (SEM), Energy dispersive X-ray spectrometer (EDX), Raman Spectroscopy (Raman), and impedance spectroscopy, respectively. The XRD result reveals that all the samples are single phase with cubic fluorite-type structure. The relative densities of samples sintered at 1400^0C are about 98% of theoretical density. The average grain sizes of YbSDC1-2 samples found from SEM image are in the range of 474-680nm. The Raman spectra result showed formation of three distinctive peaks in the YbSDC1-2 lattice. An intense peak at 464cm^{-1} and two weaker peaks at 260cm^{-1} and 552cm^{-1}. Based on impedance spectroscopy results, the composition $Ce_{0.85}Sm_{0.05}Yb_{0.1}O_{1.925}$ exhibited greater conductivity of 4.4 x10^{-3} S/cm than that of composition $Ce_{0.85}Sm_{0.05}Yb_{0.05}O_{1.95}$ which exhibited a conductivity of 1.88 x10^{-3} S/cm at 500^0C in air atmosphere. All the results confirmed that Yb and Sm co-doped ceria is a promising alternative electrolyte for intermediate temperature solid oxide fuel cell (IT-SOFC) applications.***

Keywords: IT-SOFCS, electrolyte, co-doped ceria, ionic conductivity.

I. INTRODUCTION

Solid oxide fuel cells (SOFCs) convert chemical energy directly into electrical energy with high efficiency and eco-friendly manner [1-9]. However, in spite of these advantages, SOFC still has commercialization related problems such as its cost of fabrication at high temperature and durability [10-13].

One of the strategies which is supposed to be addressed to overcome the bottle-neck of operating temperatures of SOFCs is finding an alternate solid electrolyte for intermediate temperature SOFCs (IT-SOFCs)[14-16]. Ceria based oxides are explicitly being investigated for intermediate temperature applications due to their various advantages over ZrO_2 -based materials [17- 19].

Among the various dopants of ceria studied, samaria doped ceria (SDC) has received great attention as a potential IT-SOFC electrolyte due to its high ionic conductivity [20-24]. However, literature results indicated that the single-doped ceria based oxides have limitations for its application as solid electrolytes due to the tendency of reduction of Ce^{4+} (ionic conduction) to Ce^{3+} (electronic conduction)[25,26].

Furthermore, such low temperatures (500^0C-700^0C) are not still suitable for singly doped ceria as electrolyte in SOFC due to high grain resistance [27].

Specifically, the structural, microstructure and electrical properties of single doped ceria with Yb for use as an electrolyte for IT-SOFC application were not described well (Ye, Mori et al, 2007). Moreover, a poor ionic conductivity value was reported for single doped ceria with ytterbium is (0.34x 10^{-3}S/cm at 500^0C)(M. Stojmenovic et al 2015) and samarium(1.7 x10^{-3} S/cm at 500^0C) (Amarsingh Bhabu et al, 2015) due to the aforementioned factors. It was reported in literatures that co-doping method is a novel principle to improve structural, electrical, and thermal stability of ceria-based electrolytes at intermediate temperature [28-32]. So far, there are no evident reports on the ionic conductivity properties of Yb and Sm co-doped ceria electrolyte. So, the author aimed on the preparation of co-doped ceria materials by Sol-Gel method in the $Ce_{1-x-y}Sm_xYb_yO_{2-\delta}$ $(YbSDC1-2)$, $(x = 0.05, Y = 0.05, 0.1.)$ materials to investigate its structural and electrical properties for use as an electrolyte for IT-SOFC application

ISSN: 2321-9653; IC Value: 45.98; SJ Impact Factor: 6.887
Volume 6 Issue XII, Dec 2018- Available at www.ijraset.com

II. EXPERIMENTAL

The samples with the general formula $Ce_{1-x-y}Sm_xYb_yO_{2-\delta}$ $(x = 0.05, Y = 0.05, 0.1)$ were synthesized through sol-gel method. High purity cerium (III) nitrate hexahydrate ($Ce(NO_3)_3 .6H_2O$, 99.9%, Otto, India), Samarium (III) nitrate hexahydrate ($Sm(NO_3)_3 .6H_2O$,99.9%, Otto, India) and Ytterbium (III) nitrate Pentahydrate ($Yb(NO_3)_3.5H_2O$, 99.9%, Otto, India) were used as the starting materials. Stoichiometric amounts of all nitrates were dissolved in distilled water under continuous stirring. Citric acid was added to the whole mixture of precursors in 1:1 molar ratio to maintain the total molar ratio of metal to citric acid. In order to adjust the *p*H to ≈7, ammonium hydroxide was added drop by drop to the solution.

After adjusting pH value, the whole mixture was stirred at 80^0C for 2-3h and a homogenous solution was then formed. After 2-3h, a yellowish viscous gel was formed. The gel was placed in an oven to form ash. As the gel was put in an oven, slowly the gel started to foam, swell and finally burn with glowing flints and the evolution of large amounts of gas occurred. This auto ignition was slowly propagated until the whole sample was fully burnt to produce a light yellow colored ash. Ash was calcined at 700°C for 2 h to remove the carbonaceous materials and the most stable mixed oxide phase was found. The resultant ash was ground continuously for 1h in agate mortar to get a fine homogeneous powder. The powders were pressed with the help of a hydraulic press under a pressure of 200MPa into a circular pellet (8mm in diameter and 2 mm in thickness). Finally, the pellets were sintered in furnace at 1400°C for 2h and prepared for other measurement techniques.

The structural characterization of all the sintered samples were done at room temperature using Philips X-ray Diffractometer with Cuk_α radiation (λ=1.54 A^0) operated at 40 kV and 30 mA in the 2θ range of 20–80° with a step size of 0.02 and a time for step is 2s. Experimental density was determined with Archimedes principle using xylene as a medium. Theoretical density was calculated from the molecular weight and uint cell volume (a^3). Relative density was calculated from the experimental density and theoretical density. The morphology of sintered pellet was taken by field- emission scanning electron microscope (FE-SEM, Carl Zeiss, Supra 40 VP). Raman spectra of sintered pellets were recorded at room temperature with (a confocal WITec CRM 200, Germany,$\lambda = 532nm$). AC impedance measurements were carried out on pellets coated with silver paint on both surfaces employing Auto lab impedance Analyzer in the frequency range 1Hz-1MHz and in the temperature range of 350^0C-500^0C.

III. RESULTS AND DISCUSSIONS

A. XRD Analysis

Fig. 1 shows the XRD patterns obtained from YbSDC1-2 samples that were prepared by sintering at 1400 ºC for 2 h. Eight symmetrical diffraction peaks were observed in the XRD spectra (111, 200, 220, 311, 222, 400, 331 and 420). This XRD pattern matches with standard single- phase cubic fluorite structure with space group Fm3m (JCPDS File No.:34-0394) [33-36]. Secondary peaks were not observed in the XRD pattern. The lattice parameter of the YbSDC1-2 sample increases slightly with increasing dopants content, as depicted in Table 1. This increase can be attributed to the substitution of the smaller Ce^{4+} (r = 0. 97A^0 by the larger Yb^{3+} (r = .985A^0) and Sm^{3+} (r = 1.08A^0) [37].

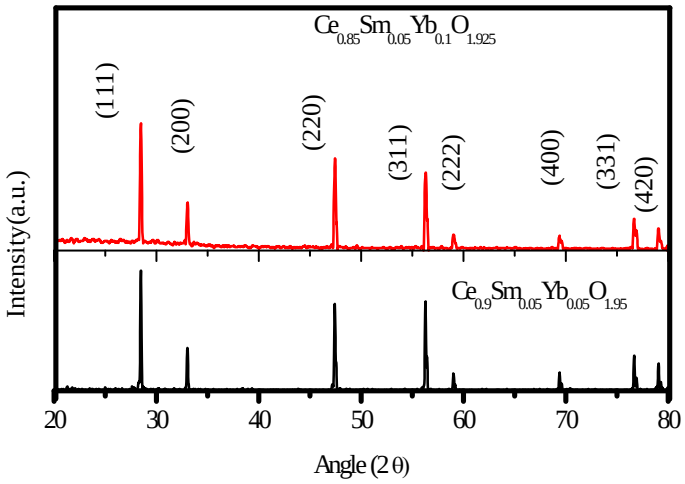

Fig.1 XRD Patterns of YbSDC1-2 Samples

The lattice parameter 'a' can be calculated from the equation:

$$a = d.\sqrt{h^2 + k^2 + l^2} \quad (1)$$

where, 'd' the inter planner distance and '*hkl*' are the Miller indices of the plane obtained in XRD measurement. Using Eq.1, the lattice parameters of YbSDC-1 and YbSDC-2 calculated were 0.5417 *nm* and 0.5419*nm* respectively and depicted in Table1. These values are slightly larger than lattice parameter of pure CeO_2 (0.5411 *nm*) [38], as expected from the effective ionic radii of Yb^{3+} and Sm^{3+} (0.10325*nm*).

In this study, the density measurement was carried out to determine the extent of porosity in prepared samples. Theoretical density was calculated using the formula which is given as [39]:

$$D_t = \frac{4}{N_A a^3}[(1-x)M_A + xM_B + (2-0.5x)M_O] \quad (2)$$

Where, '*x*' is the average mass of samarium and ytterbium content, '*a*' the lattice parameter at room temperature of samples, N_a the Avogadro number ($6.023x10^{23}$), M_A, M_B, and M_O refers atomic weights of cerium, average weights of samarium and ytterbium, oxygen respectively.

The relative density η is calculated as a relation in percentage of the sample density (D_e) to the theoretical density (D_t):

$$\eta = \frac{D_e}{D_t} x\ 100\% \quad (3)$$

The theoretical, experimental and relative densities of YbSDC1-2 samples were shown in Table1. As it can be observed from Table1, the calculated relative densities of YbSDC1-2 samples were about 98% of the theoretical densities and these findings were supported by SEM images.

Table 1.Grain size, lattice parameter and relative densities of YbSDC1-2 samples.

No.	Compositions	Grain size (*nm*)	Lattice parameter (*nm*)	Theoretical Density (g/cm3)	Experimental Density(g/cm3)	Relative density (%)
1	$Ce_{0.9}Sm_{0.05}Yb_{0.05}O_{1.95}$	474	0.5417	7.28938	7.17825	98.5
2	$Ce_{0.85}Sm_{0.05}Yb_{0.1}O_{1.925}$	680	0.5419	7.42467	7.3292	98.7

B. SEM and EDX Analysis

The morphology and chemical composition of YbSDC-1 and YbSDC-2 samples presented in Fig.2 and Fig.3 respectively. SEM micrograph clearly shows the presence of uniform grains with clean and distinct grain boundaries. It can be seen that the surface of the samples shows high densification with few invisible pores indicating relative density less than 100%. As shown in Table 1, The average grain sizes of YbSDC1-2 samples found from SEM image are in the range of 474-680nm. In this study, average grain size of all the samples was calculated by linear intercept technique. It also depicts that the grain sizes of YbSDC1-2 samples increased with proportion of ytterbium. This finding is consistent with the result reported in the previous literature [40]. It can be seen from Fig.3, the EDX graph confirmed the presence of elements Yb, Sm, Ce and O in the YbSDC1-2 samples and no other elements were observed. Moreover, Fig.3, indicated the atomic weight of elements Yb, Sm, Ce and O found in each sample is as per stochiometry.

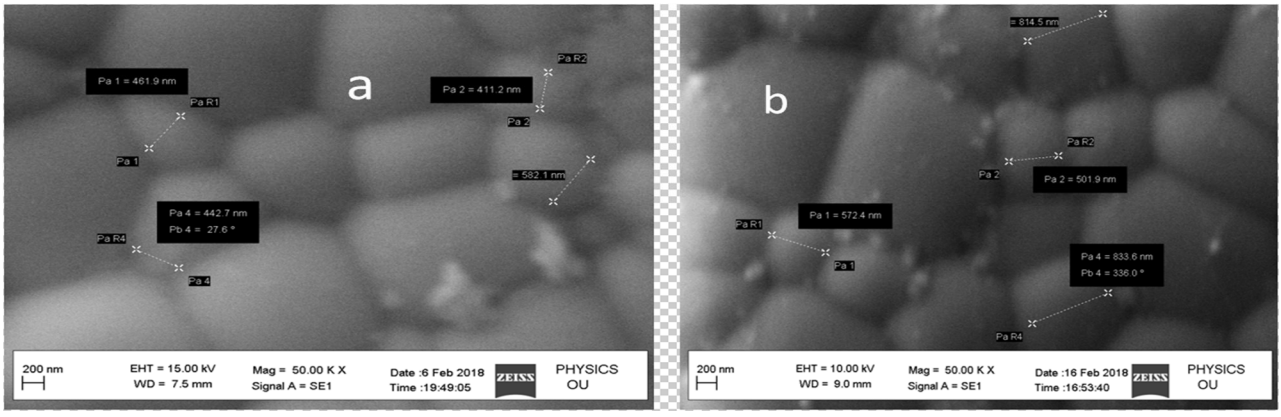

Fig.2. SEM graphs of (a) $Ce_{0.9}Sm_{0.05}Yb_{0.05}O_{1.95}$ (b) $Ce_{0.85}Sm_{0.05}Yb_{0.1}O_{1.925}$

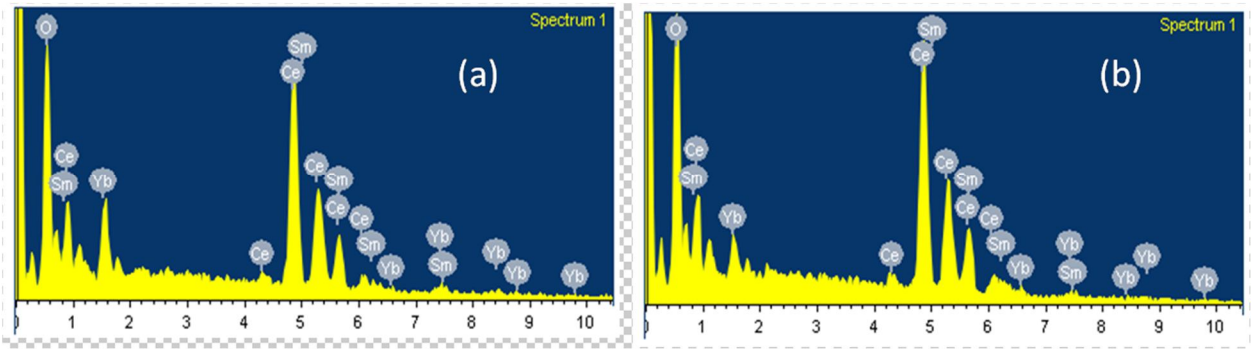

Fig.3.EDX analysis of (a) $Ce_{0.9}Sm_{0.05}Yb_{0.05}O_{1.95}$ (b) $Ce_{0.85}Sm_{0.05}Yb_{0.1}O_{1.925}$

C. Raman Spectroscopy

Fig. 4 shows the in situ Raman spectra of the $Ce_{0.9}Sm_{0.05}$ $Yb_{0.05}O_{1.95}$ and$Ce_{0.85}Sm_{0.05}Yb_{0.1}O_{1.925}$ samples sintered at 1400^{0}C. It can be seen that each Raman spectrum consists of three distinctive peaks. The strong intensive peak observed at 464 cm^{-1} is attributed to first order Raman mode with F_{2g} symmetric vibration of ceria cations surrounded by oxygen anions, which confirms the formation of YbSDC1-2 solid solution [41, 42]. The second weak peak observed at 260cm^{-1} can be assigned to the higher order modes of ceria, namely to the second order transverse acoustic mode, that is, 2TA [43-45]. The second weak peak appeared at 552 cm^{-1} is due to the oxygen vacancy created by the replacement of Ce^{4+} with Sm^{3+} and Yb^{3+} in order to maintain the charge neutrality in the lattice. This band became stronger with increasing Yb^{3+} content in the YbSDC1-2 samples.

Recently, it was reported that the concentration of oxygen vacancies in ceria can be calculated by the intensity ratio of strong intense peak to the weak intense peak (i.e. I_{552}/I_{464}). It is also reported that the oxygen vacancy concentration in ceria solid solution can be estimated by the ratio of area of strong peak to the area of weak peak (i.e. A_{552}/A_{464}) [46-48]. In the present study, the values of intensity ratios (i.e. I_{552}/I_{464}) found for YbSDC-1 and YbSDC-2 are 0.10 and 0.13 respectively.

The higher value of I_{552}/I_{464} or YbSDC-2 than YbSDC-1 confirmed that the formation of higher concentration of oxygen vacancies which causes the mobilization of ions in the ceria lattice resulting in better total ionic conductivity with less activation energy. In this study, the Raman observation confirms the formation of single phase YbSDC1-2 solid material supporting X-ray diffraction patterns indicated in Fig.1.

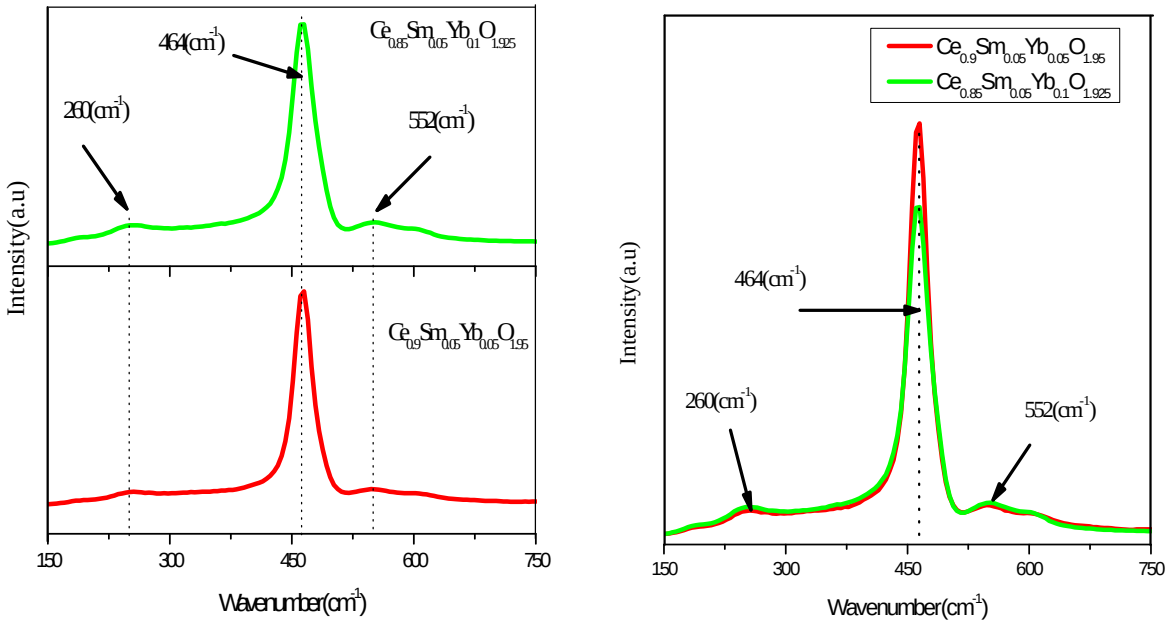

Fig.4. Raman spectra of YbSDC1-2 samples sintered at 1400^{0}C.

D. Impedance Spectroscopy

Impedance plots of YbSDC1-2 samples recorded at different temperatures are shown in Fig. 5a-d. In this work, the equivalent circuit model used to fit the impedance spectra was represented as a series connection of three parts. This includes the grain resistance *R*g, the parallel connection of grain boundary resistance *R*gb and grain boundary constant phase element (*C*PE1), and the parallel connection of electrode resistance *R*e and constant phase element (*C*PE2).

The impedance spectra collected showed an arc for grain boundary resistance and incomplete depressed arc for electrode resistance behavior only as shown in Fig.5a-d. However, the arc in the high frequency range which represents the grain resistance is not displayed because of the limited frequency of measuring equipment (1 Hz -1 MHz). Starting from the origin, the arc was not displayed for high frequency range. This length of real axis for which the arc is not displayed represented as the grain resistance. This behavior of impedance was also reported for doped ceria in previous literatures [49-53].

The grain resistance (Rg) was represented with the left horizontal axis (arc is not displayed), whereas Rgb was determined from fitting medium frequency arc intercept on the real axis.

The total resistance is given by

$$R = R_g + R_{gb} \quad (4)$$

Where *R*g and *R*gb stand for the resistance of grain interior and grain boundary respectively.

Then, the ionic conductivity (σ) of each sample was calculated using the equation:

$$\sigma = \frac{l}{RA} \quad (5)$$

where l is the thickness of sample and A is the cross-sectional area. Through fitting the data and using Eqs. (4) and (5), the ionic conductivities of samples at different temperatures was obtained. This result is presented in Table 2 & 3.

Table 2. Rg, Rgb, R and Conductivities of $Ce_{0.9}Sm_{0.05}Yb_{0.05}O_{1.95}$ at different measuring temperatures.

Temperature(^{0}C)	$Rg(\Omega$	$Rgb(\Omega$	$R(\Omega$	$\sigma(S/cm)$
300	548.76	27163.29	27712.05	$2.58x10^{-5}$
350	297.58	8826.22	9123.8	$7.82x10^{-5}$
400	98.99	2547.5	2646.49	$2.69x10^{-4}$
450	50.32	962.38	1012.70	$7.05x10^{-4}$
500	28.52	351.02	379.54	$1.88x10^{-3}$

Table 3.Rg, Rgb, R and conductivities of $Ce_{0.85}Sm_{0.05}Yb_{0.1}O_{1.925}$ at different measuring temperatures.

Temperature(^{0}C)	$Rg(\Omega$	$Rgb(\Omega$	$R_T(\Omega$	$\sigma(S/cm)$
300	567.58	10219.21	10786.79	$6.62\ x10^{-5}$
350	353.74	3133.13	3486.87	$2.04\ x10^{-4}$
400	140.79	957.11	1097.9	$6.5\ x10^{-4}$
450	75.37	329.8	405.17	$1.76\ x10^{-3}$
500	46.64	115.64	162.28	$4.4\ x10^{-3}$

As shown in Table 2 and 3, the grain boundary resistance of YbSDC-2 sample was dramatically decreased compared with that of YbSDC-1 with rise in measuring temperature. This shows that increase in the amounts of Yb with constant Sm concentration has significant effect on the decrease of the grain boundary resistance. It was observed in Table1, the grain size ofYbSDC-2 sample is larger than that of YbSDC-1.The larger the grain size, the smaller grain-boundary region which resulted in the smaller grain boundary resistance and total resistance of the sample. Consequently, this resulted in the greater conductivity of YbSDC-2 sample than that of YbSDC-1. The increase in conductivity with increase in grain size is supported with the results reported in previous literatures [52]. Moreover, the increase in conductivity with increase in ytterbium doping is consistent with the results reported previously for single Yb doped ceria [51].

As indicated in Table 2 & 3, the conductivity of composition $Ce_{0.85}Sm_{0.05}Yb_{0.1}O_{1.925}$ found is 4.4 $x10^{-3}$ S/cm whereas that of composition $Ce_{0.85}Sm_{0.05}Yb_{0.05}O_{1.95}$ obtained is 1.88 $x10^{-3}$ S/cm at 500^{0}C in air atmosphere. That is, the conductivity of $Ce_{0.85}Sm_{0.05}Yb_{0.1}O_{1.925}$ is two times that of $Ce_{0.9}Sm_{0.05}Yb_{0.05}O_{1.95}$.

As reported in literatures, the grain and grain boundary arcs of doped ceria electrolytes are associated with the capacitances in the 30 to 60*pF* and 7 to 25*nF* ranges respectively [54-55]. These are determined from the relation $2\pi f_{max}RC=1$, where f_{max} is the applied frequency at the arc maximum, R is the resistance, and C is the capacitance of a particular contribution.

In this study, the values of Cgb calculated for the middle range frequency semicircles obtained at 450^{0}C (Fig.5c) and at 500^{0}C (Fig.5d) are 36.64*nF*, 31.65*nF* for YbSDC-1 and 9.6*nF*, 9.36*nF* for YbSDC-2 respectively. The calculated values of Cgb found are almost close to the expected values for grain boundary response. This confirmed that the middle range frequency semicircle in the impedance spectra measured at 450 and 500^{0}C in YbSDC1-2 samples is almost associated with the grain boundary resistance.

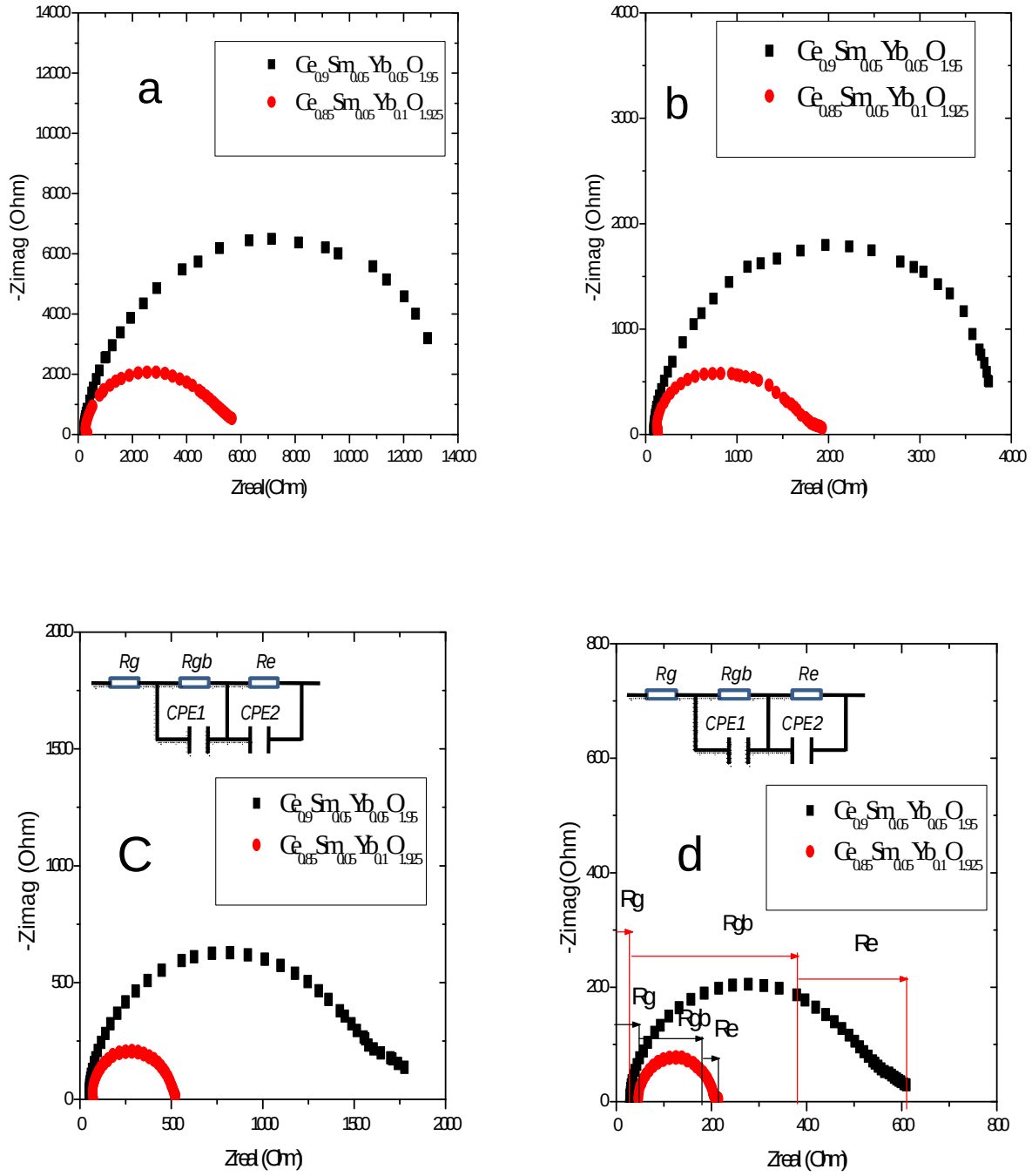

Fig. 5 Impedance plots of YbSDC1-2 samples measured in air at (a) 350^{o}C (b) 400 ^{0}C (c) 450 ^{0}C and (d) 500 ^{0}C.

The temperature dependence of ionic conductivity often follows an Arrhenius relation:

$$\sigma T = \sigma_o e^{Ea/kT} \quad (6)$$

where *Ea* is the activation energy for conduction, *T* is the absolute temperature, *k* is the Boltzmann's constant and σ_o is a pre-exponential factor. The total ionic conductivities of YbSDC1-2 samples sintered at 1400^0C for 2h was presented in Fig.6 in the form of $\ln(\sigma T)$ versus$\left(10^3/T\right)$. The value of *Ea* and σ_o were found from the slope and intercept of the graph respectively.

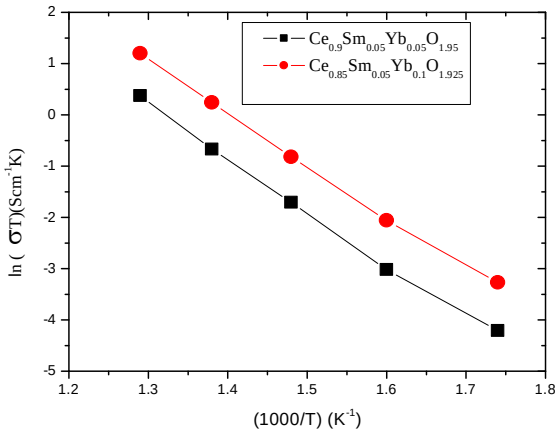

Fig.6. Arrhenius plots of total conductivity of $Ce_{0.9}Sm_{0.05}Yb_{0.05}O_{1.95}$ and $Ce_{0.85}Sm_{0.05}Yb_{0.1}O_{1.925}$ samples

The Arrhenius plot described in Fig. 6, reveals that the conductivity of YbSDC1-2 samples increased linearly with temperature. Moreover, the plot indicated that the conductivity of YbSDC-2 sample is greater than that of YbSDC-1. This could be due to formation of more number of oxygen vacancies and suppression of ordering of oxygen vacancies in YbSDC-2 than in YbSDC-1 which leads to a decrease in the activation energy for diffusion of O^{2-} ions.

The Arrhenius plots of YbSDC1-2 samples showed a change in the slope at 350°C.This indicates that a transition from associated defect pairs (regions where oxygen vacancies are bound to cation defects to dissociated defects (regions where oxygen vacancies are free).

Table 4.shows that the activation energy of YbSDC1-2 samples obtained by fitting of the data in Fig.6. to Arrhenius relations (eq.6).

Table 4. Activation energy of YbSDC1-2 system obtained by slope fitting.

No	Sample	Ea(*eV*)
1	$Ce_{0.9}Sm_{0.05}Yb_{0.05}O_{1.95}$	0.93
2	$Ce_{0.85}Sm_{0.05}Yb_{0.1}O_{1.925}$	0.92

Literature result indicated that for the lanthanide series, the combinations of rare earth dopants producing an average atomic number between 61 and 62 should be the right choice to get the lowest activation energy (Ea) in doped ceria [57]. In this regard, the combinations of Nd/Sm and Pr/Gd show low activation energy and enhanced ionic conductivity.

As it can be observed in Table 4, the activation energy of Yb and Sm codoped ceria reported in this work is smaller than single doped ceria with Yb (1.18eV) and greater than single doped ceria with Sm(0.76eV) reported in previous literatures [38,51]. This is possibly due to improvement in the dopants (Sm/Yb) average atomic number (66) which is closer to the ideal dopants effective atomic number 61(Pm) and 62(Sm) than that of Yb (70) atomic number. Moreover, it may be due to increase in the effective ionic radii of co dopants which is close to the critical ionic radii (0.1038nm) for doped ceria [58]. As the ionic radii of dopant cations is closer to critical ionic radii of host, the lower activation energy effect to the diffusion of oxygen vacancies and the greater the conductivity of the electrolyte. Therfore, the above result indicated that co-doping Yb and Sm in ceria lowered activation energy and enhanced its electrical properties. Moreover, the conductivity of codoped YbSDC1-2 samples obtained at 500^0C in this work was greater than that of single doped ceria with Yb previously reported literatures [16, 56]. The results confirmed that co-doping method of Yb and Sm increases the conductivity of ceria at intermediate temperature.

IV. CONCLUSION

Ytterbium and Samarium co-doped ceria samples were successfully prepared through sol-gel method. In order to obtain dense ceramics, the sample pellets were sintered at 1400^0C for 2h. The XRD result reveals that all the samples are single phase with cubic fluorite-type structure. The calculated relative densities were about 98% of the theoretical densities. SEM micrograph clearly showed the presence of uniform grains with clean and distinct grain boundaries. The EDX graph reveals that all elements like Yb, Sm, Ce and O_2 are entered in the lattice as per stochiometry. The Raman spectra result showed three distinctive peaks. An intense peak at 464cm^{-1} and two weaker peaks at 260cm^{-1} and 552cm^{-1}. Raman spectroscopy analysis showed that the values of intensity ratios (i.e. I_{552}/I_{464}) found for YbSDC-1 and YbSDC-2 are 0.10 and 0.13 respectively. The conductivity of YbSDC1-2 increased with the increase in the ytterbium substitution with constant samarium dopant. The composition $Ce_{0.85}Sm_{0.05}Yb_{0.1}O_{1.925}$ showed higher ionic conductivity and minimum activation energy of (4.4 x10^{-3}S/cm, Ea = 0.92eV) than composition $Ce_{0.85}Sm_{0.05}Yb_{0.1}O_{1.925}$ which showed a conductivity and activation energy of (1.88 x10^{-3}S/cm, Ea = 0.93eV) respectively at 500^0C in air atmosphere. From the experimental results, all YbSDC1-2 samples showed conductivity higher than 10^{-3}S/cm at temperature of 500^0C. Therefore, the results confirmed that the material prepared from $Ce_{1-x-y}Sm_xYb_yO_{2-\delta}$ (x = 0.05, Y = 0.05,0.1) can be used as an electrolyte for intermediate temperature SOFC applications.

V. ACKNOWLEDGEMENT

The authors are very much thankful to Material Research Laboratory, Department of Physics, Osmania University, and Hyderabad, India for giving opportunity to do experimental work. Also, the authors thank Department of Physics, Wollega University, Ethiopia for providing financial support to visit Osmania University, Hyderabad, India.

REFERENCES

[1] Shajahana, J. Ahnb, P. Naira, S. Medisettia, S. Patila,V. Nivedithaa, G. U. B. Babuc, H. P.Dasaria, J.H. Leeb, Praseodymium doped ceria as electrolyte material for IT-SOFC applications, Mater. Chem. Phys. 2016(2018) 136-142.
[2] Y. Gan, J. Cheng, M. Li, H. Zhan, W. Sun, Enhanced ceria based electrolytes by codoping samaria and Scandia for intermediate temperature solid oxide fuel cells, Mater. Chem. Phys. 163(2015) 279-285.
[3] A. S. Kumar, R. Balaji, S. Jayakumar, C. Pradeep, Microwave assisted sintering of gadolinium doped barium cerate electrolyte for intermediate temperature solid oxide fuel cells, Mater. Chem. Phys. 182(2016) 520-525.
[4] A. S. Kumar, R. Balaji, S. Jayakumar, Thermal, structural and electrical properties of samarium doped barium cerate electrolyte for SOFCs, Mater. Chem. Phys. 202(2017) 82-88.
[5] S. Kobi, N. Jaiswal, D. Kumar, O. Parkash, Ionic conductivity of Nd^{3+} and Y^{3+} co-doped ceria solid electrolytes for intermediate temperature solid oxide fuel cells, J. Allo. Comp. (2015).
[6] K. Venkataramana, C. Madhuri, Y. S. Reddy, G. Bhikshamaiah, C. V. Reddy, Structural, electrical and thermal expansion studies of tri-doped ceria electrolyte materials for IT-SOFCs, J. Allo. Comp. (2017).
[7] C. E. Jeyanthi, R. Siddheswaran, P. Kumar, M. K. Chinnu, K. Rajarajan, R. Jayavel, Investigation on synthesis, structure, morphology, spectroscopic and electrochemical studies of praseodymium-doped ceria nanoparticles by combustion method, Mater. Chem. Phys.151 (2015) 22-28.
[8] G. Donmez, V. Sarıboga, T. G. Altıncekic , M. A. Faruk Oksuzomer, Polyol Synthesis and Investigation of $Ce_{1-x}RE_xO_{2-x/2}$ (RE = Sm, Gd, Nd, La,0 ≤ x ≤ 0.25) Electrolytes for IT-SOFCs, J.. Am. Ceram. Soc. (2014) 1–9.
[9] Damisih, J. Raharjo, Masmui, R. S. Aninda, N. A. Lestari, Synthesis and Characterization of La, Sc, Yb and Nd codoped Gadolinium doped Cerium (GDC) Composite Electrolyte for IT-SOFC, Journal of Physics: Conf. Series 877 (2017) 012077.
[10] M. Choolaeia, Q. Caia, Robert C.T. Sladeb, B. A. Horria, Nanocrystalline gadolinium-doped ceria (GDC) for SOFCs by an environmentally-friendly single step method, Ceram. Int. 44 (2018) 13286–13292.
[11] S. Ramesh, K.C. J. Raju, Preparation and characterization of $Ce_{1-x}(Gd_{0.5}Pr_{0.5})_xO_2$ electrolyte for IT-SOFCs, int. J. hydrogen energy 37(2012)10311-10317.
[12] Z. Shao, W. Zhou, Z. Zhu, Advanced synthesis of materials for intermediate-temperature solid oxide fuel cells, Progress in Mat. Sci. 57 (2012) 804–874.
[13] Y. Xia, X. Liu, Y. Bai, H. Li, X. Deng, X. Niu, X. Wu, D. Zhou, Z. Wang, J. Meng, Electrical properties optimization of calcium Co-doping system: $CeO_2Sm_2O_3$, Int.J. hydrogen energy 37(2012)11934-11940.
[14] J. Molenda, K. Swierczek, W. Zaj, Functional materials for the IT-SOFC, J. Power Sources 173 (2007) 657–670.
[15] S. Omar, E. D. Wachsman, J. C. Nino, Higher ionic conductive ceria-based electrolytes for solid oxide fuel cells, Appl. Phys. Lett. 91, 144106 (2007); doi: 10.1063/1.2794725.
[16] A. Tarancón, Strategies for Lowering Solid Oxide Fuel Cells Operating Temperature, Energies 2 (2009)1130-1150; doi: 10.3390/en20401130.
[17] G. Kim, N. Lee , K.B. Kim, B. K. Kim, H. Chang, S.J. Song, J.Y. Park, Various synthesis methods of aliovalent-doped ceria and their electrical properties for intermediate temperature solid oxide electrolytes, Int.J.Hydrogen energy 38(2013)1571-1587.
[18] L. Spiridigliozzi, G. Dell'Agli, A. Marocco, G.Accardo, C. Ferone, R. Cioffi, Hydrothermal synthesis at low temperature gadolinium doped ceria, Proceedings of EFC2015.
[19] G. Accardo, C. Ferone, R. Ciof, D.Fratni, L. Spiridigliozzi, G. Dell'Agli, Electrical and microstructural characterizaton of ceramic gadolinium-doped ceria electrolytes for ITSOFCs by sol-gel route, J .Appl. Biomater. Funct.Mater.14(1)(2016) e35-e41, DOI: 10.5301/jabfm.5000265.
[20] P. C. C. Dazaa, R. A. M. Menesesa, A. C. M. Rodrigues, C. R. M. Silvaa, Ionic conductivities and high resolution microscopic evaluation of grain and grain boundaries of cerium-based codoped solid electrolytes, Ceram. Int. 44 (2018) 13699–13705.

[21] T. Karaca, T. G.Altıncekic¸M. Faruk. Oksuzomer, Synthesis of nanocrystalline samarium-doped CeO2 (SDC) powders as a solid electrolyte by using a simple solvothermal route, Ceram. Int. 36 (2010) 1101–1107.
[22] M. R. Kosinski, R. T. Baker, Preparation and property–performance relationships in samarium-doped ceria nanopowders for solid oxide fuel cell electrolytes, J. Power Sources 196 (2011) 2498–2512.
[23] A. Arabaci, Effect of Sm and Gd dopants on structural characteristics and ionic conductivity of ceria, Ceram. Int.41 (2015) 5836–5842.
[24] G. Dell'Aglia, L. Spiridigliozzia, A. Maroccoa, G. Accardoc, D. Frattinid, Y. Kwond, S.P. Yoon, Morphological and crystalline evolution of Sm-(20 mol%)–doped ceria nanopowders prepared by a combined co-precipitation/hydrothermal synthesis for solid oxide fuel cell applications, Ceram. Int.43 (2017) 12799–12808.
[25] Y.Ch. Wu, C.C. Lin, The microstructures and property analysis of aliovalent cations (Sm^{3+}, Mg^{2+}, Ca^{2+}, Sr^{2+}, Ba^{2+}) co-doped ceria-base electrolytes after an aging treatment, Int. J. hydrogen energy 39(2014)7988-8001.
[26] Sandhya K, Chitra Priya N. S., Aswathy P K, D. N Rajendran, impact of reduced sintering temperature on the grain size of samarium doped ceria electrolyte, Int.J.journal of Advance Research in Science and Engineering 6(2017).
[27] N. K. Singh, P. Singh, D. Kumar, O. Parkash, Electrical conductivity of undoped, singly doped, and co-doped ceria , Ionics18 (2012) 127–134 , DOI 10.1007/s11581-011-0604-9 .
[28] B. Li, Y. Liu, X. Wei, W. Pan, Electrical properties of ceria Co-doped with Sm^{3+} and Nd^{3}, J. Power Sources 195 (2010) 969–976.
[29] B. Suresh M, J. Roy, The effect of strontium doping on densification and electrical properties of $Ce_{0.8}Gd_{0.2}O_{2-\delta}$ electrolyte for IT-SOFC application, Ionics, 18(2012) 291–297, DOI 10.1007/s11581-011-0633-4.
[30] S. Ramesh, K. C. J.Raju, C. V. Reddy, Preparation and characterization of $Ce_{1-x}Dy_{x-y}SryO_{2-\delta}$ system, Trans. Nonferrous Met. Soc. China 24(2014) 393-400.
[31] Y.C. Wua, C.H. Chiena, G. Xu, Conductivity and microstructure analysis of ceria materials doped with multiple elements, Ceram. Int. 43 (2017) S747–S757.
[32] W. Zając, J. Molenda, Electrical conductivity of doubly doped ceria, Solid State Ionics179 (2008) 154–158.
[33] K.C. Anjaneya, M. P. Singh, Synthesis and properties of gadolinium doped ceria electrolyte for IT-SOFCs by EDTA-citrate complexing method, J. Allo. Comp. 695 (2017) 871e876.
[34] K. A. Bhabu, J. Theerthagiri, J. Madhavan, T. Balu,G. Muralidharan, T. R. Rajasekaran, Cubic fluorite phase of samarium doped cerium oxide $(CeO_2)_{0.96}Sm_{0.04}$ for solid oxide fuel cell electrolyte, J Mater Sci: Mater Electron, DOI 10.1007/s10854-015-3925-z.
[35] M. Kahlaouin, S. Chefi, A. Inoubli, A. Madani, C. Chefi, Synthesis and electrical properties of co-doping with La^{3+}, Nd^{3+}, Y^{3+}, and Eu^{3+} citric acid-nitrate prepared samarium-doped ceria ceramics, Ceram. Int.39 (2013) 3873–3879.
[36] G. Accardoa, D. Frattinib, H.C. Hama, J.H. Hanc, S.P. Yoon, Improved microstructure and sintering temperature of bismuth nano-doped GDC powders synthesized by direct sol-gel combustion, Ceram. Int. 44 (2018) 3800–3809.
[37] M. Stojmenovic, M. Zunic, J. Gulicovski, D. Bajuk-Bogdanovic, H. Antunovic, V. Dodevski1, S. Mentus, Structural, morphological, and electrical properties of doped ceria as a solid electrolyte for intermediate-temperature solid oxide fuel cells, J Mater Sci (2015) 50:3781–3794, DOI 10.1007/s10853-015-8943-y.
[38] M.L. Dos Santos, R.C. Lima, C.S. Riccardi, R.L. Tranquilin, P.R. Bueno, J.A. Varela, E. Longo, Preparation and characterization of ceria nanospheres by microwave-hydrothermal method, Materials Letters 62 (2008) 4509–4511.
[39] J. Yang, B. Ji, J. Si, Q. Zhang, Q.Yin, J. Xie, C. Tian, Synthesis and properties of ceria based electrolyte for IT-SOFCs, Int. J. hydrogen energyy41(2016015979-15984.
[40] F. Ye, T. Mori, D .Rong Ou, M.Takahashi, J. Zou, J. Drennanc, Ionic Conductivities and Microstructures of Ytterbium-Doped Ceria, J. Electrochem. Soci. 154 (2007)2 B180-B185.
[41] M. Guo, J. Lu, Y. Wu, Y.Wang, M. Luo, UV and Visible Raman Studies of Oxygen Vacancies in Rare-Earth-Doped Ceria, Langmuir 27(2011) 3872–3877, dx.doi.org/10.1021/la200292f.
[42] A. Filtschew, K. Hofmann, C. Hess, Ceria and Its Defect Structure: New Insights from a Combined Spectroscopic Approach, Phys. Chem. C120(2016) 6694-6703, DOI: .1021/acs.jpcc.6b00959.
[43] E.Swatsitang, S. Phokha, S. Hunpratub, S. Maensiri, Modification of Ce valence states by Sm/Sr co-doping of CeO_2 nanoparticles for improved magneto-electrochemical properties, Materials and Design 108 (2016) 27–33.
[44] M. Piumetti, S. Bensaid, T. Andana, M. Dosa, C. Novara, F. Giorgis, N. Russo, D. Fino, Nanostructured Ceria-Based Materials: Effect of the Hydrothermal Synthesis Conditions on the Structural Properties and Catalytic Activity, Catalysts 7(2017) 174; doi:10.3390/catal7060174.
[45] J. E. Spanier, R. D. Robinson, F. Zhang, S.W.Chan, I. P. Herman, Size-dependent properties of $CeO_{2-\delta}$ nanoparticles as studied by Raman scattering, Phys.Review B, 64, 245407, DOI: 10.1103/PhysRevB.64.245407.
[46] S.P. Li, J.Q. Lu, P. Fang, M.F.Luo, Effect of oxygen vacancies on electrical properties of $Ce_{0.8}Sm_{0.1}Nd_{0.1}O_{2-\delta}$ electrolyte: An in situ Raman spectroscopic study, J. Power Sources 193 (2009) 93–98.
[47] J. M. López, A. L. Gilbank, T. García, B. Solsona, S. Agouram, L. T. Murciano, The prevalence of surface oxygen vacancies over the mobility of bulk oxygen in nanostructured ceria for the total toluene oxidation, Appl. Catal. B: Environmental 174–175 (2015) 403–412.
[48] Z.Y. Pu, J.Q. Lu, M. F. Luo, Y. L. Xie, Study of Oxygen Vacancies in $Ce_{0.9}Pr_{0.1}O_{2-\delta}$ Solid Solution by in Situ X-ray Diffraction and in Situ Raman Spectroscopy, J. Phys. Chem. C 2007, 111, 18695-18702.
[49] A. A. Jaisa, S.A. M. Alia, M. Anwara, M. R. Somalua, A. Muchtara, W. Wan Isahakc, C. Y. Tand, R. Singhd, N. P. Brandone, Enhanced ionic conductivity of scandia-ceria-stabilized-zirconia (10Sc1CeSZ) electrolyte synthesized by the microwave-assisted glycine nitrate process, Ceram. Int. 43 (2017) 8119–8125.
[50] S.A. Muhammed Alia, Mustafa Anwara,b, Abdalla M. Abdallac, Mahendra Rao Somalua, Andanastuti Muchtar, $Ce_{0.80}Sm_{0.10}Ba_{0.05}Er_{0.05}O_{2-\delta}$ multi-doped ceria electrolyte for intermediate temperature solid oxide fuel cells, Ceramics International 43 (2017) 1265–1271.
[51] B. Matovic, M. Stojmenovic, J. Pantic, A. Varela, M. Zuni, N. Jiraborvornpongsa, T. Yano, Electrical and microstructural properties of Yb-doped CeO_2, J. Asian Ceram. Soci. (2014).
[52] L. Xiaomin, L.Ü. Qiuyue, Z. Lili, L. Xiaomei, Synthesis and characterization of $Ce_{0.8}Sm_{0.2-x}Pr_xO_{2-\delta}$ (x=0.02–0.08) solid electrolyte materials,J.Rare Earths 33(2015)4.
[53] V. Singh1, S.Babu, A. S. Karakoti, A. Agarwal, S. Seal, Effect of Submicron Grains on Ionic Conductivity of Nanocrystalline Doped Ceria, J. Nanoscience and Nanotechnology 10(2010)1-9.

[54] D. Bucevaca, A. Radojkovic, M. Miljkovicc, B. Babica, B. Matovic, Effect of preparation route on the microstructure and electrical conductivity of co-doped ceria, Ceram. Int.39 (2013) 3603–3611.

[55] N. Jaiswal, D. Kumar, S. Upadhyay, O. Parkash, Preparation and characterization of $Ce_{0.85}La_{0.15-x}Sr_xO_{\{2-(0.075+x/2)\}}$ solid electrolytes for intermediate temperature solid oxide fuel cells, Ionics (2015) 21:497–505, DOI 10.1007/s11581-014-1190-4.

[56] F. Y. Wang, B.Z. Wan, S. Cheng, Study on Gd^{3+} and Sm^{3+} co-doped ceria-based electrolytes, J.Solid State Electrochem 9(2005) 168–173, DOI 10.1007/s10008-004-0575-0.

[57] D. A. Andersso, S. I. Simak, N. V. Skorodumova, I. A. Abrikosov, B. Johansson, Optimization of ionic conductivity in doped ceria, PNAS 13(2006) 10.

[58] S. Omar, E. D. Wachsman, J. L. Jones, J.C. Nino, Crystal Structure–Ionic Conductivity Relationships in Doped Ceria Systems, J. Am. Ceram. Soc., 92 [11](2009) 2674–2681, DOI: 10.1111/j.1551-2916.2009.03273.x.

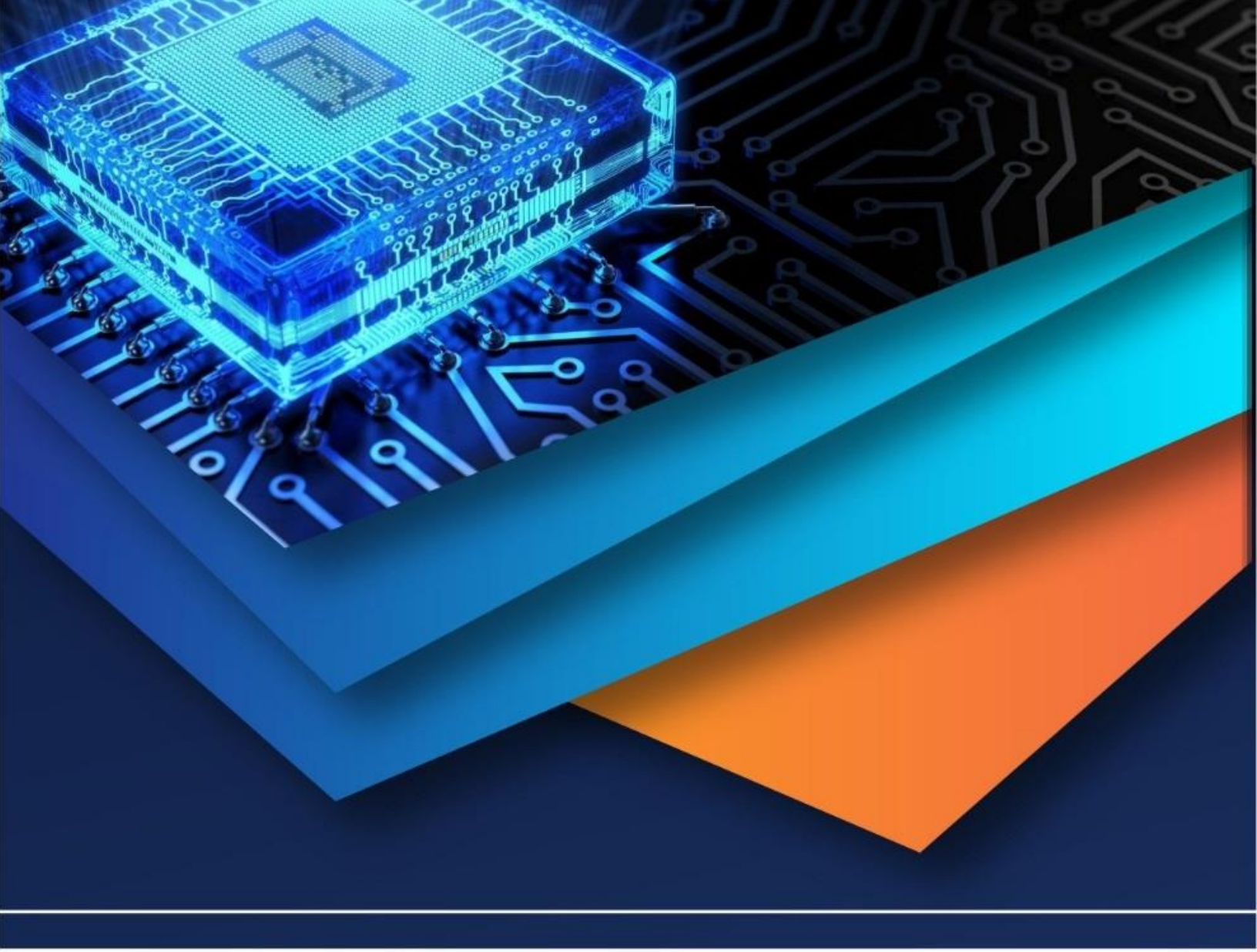

10.22214/IJRASET

45.98

IMPACT FACTOR: 7.129

IMPACT FACTOR: 7.429

INTERNATIONAL JOURNAL FOR RESEARCH

IN APPLIED SCIENCE & ENGINEERING TECHNOLOGY